Granular Matter (2013) 15:583–593
DOI 10.1007/s10035-013-0422-z

ORIGINAL PAPER

Density dependent macro-micro behavior of granular materials in general triaxial loading for varying intermediate principal stress using DEM

Md. Mahmud Sazzad · Kiichi Suzuki

Received: 14 July 2012 / Published online: 24 May 2013

Abstract This study presents the density dependent behavior of granular materials for varying intermediate principal stress (σ_2) in general triaxial loading using the discrete element method (DEM). The variation of intermediate principal stress is represented by a non-dimensional parameter $b[= (\sigma_2 - \sigma_3)/(\sigma_1 - \sigma_3)]$, where σ_1 and σ_3 are the major and minor principal stresses, respectively. Isotropically compressed dense and loose samples were prepared numerically using the periodic boundaries. The numerical dense and loose samples were subjected to shear deformation under strain controlled condition for different b values ranging from 0 to 1. The simulated macro results depict that the friction angle increases with b until it reaches a peak value and beyond the peak, the friction angle decreases with b regardless of the density of sample. A unique relationship between dilatancy index and equivalent deviatoric strain exists at small strain level for different b values when dense sample is considered. By contrast, the same relationship for loose sample does not show uniqueness. The relationships among the major, intermediate and minor principal strains depict non-linear behavior. The non-linearity is dominant for loose sample. The fluctuation in the evolution of strain increment vector direction is dominant in loose sample than dense sample. The evolution of different micro results is presented as well. It is noted that a unique relationship exists between the stress ratio and the fabric measure regardless of b and the density of sample when strong contacts are considered.

Md. M. Sazzad (✉)
Department of Civil Engineering, Rajshahi University of Engineering and Technology, Rajshahi 6204, Bangladesh
e-mail: mmsruet@gmail.com

K. Suzuki
Department of Civil and Environmental Engineering, Saitama University, Saitama 338-8570, Japan

Keywords Discrete element method · Density · b value · Micro-response

1 Introduction

The term b represents the relative magnitude of the intermediate principal stress with respect to the major and minor principal stresses and is expressed as $b = (\sigma_2 - \sigma_3)/(\sigma_1 - \sigma_3)$, where σ_1, σ_2 and σ_3 represent the major, intermediate and minor principal stresses, respectively. Habib [1] was probably the first to introduce the term b rather than σ_2 and subsequently, numerous experimental studies have been devoted to investigate the effect of b under different conditions (e.g., [2–7]). The experimental studies depict that the friction angle $\phi = \sin^{-1}[(\sigma_1 - \sigma_3)/(\sigma_1 + \sigma_3)]$ increases from $b = 0$ (axisymmetric triaxial compression) to a certain b value and beyond the peak, ϕ either decreases or increases or even remains constant as b increases. These ambiguities may be because of the type of soil, testing conditions, boundary conditions and instrumental limitations. They may also be partly due to the variation of the initial fabric of the tested samples in experimental based studies, because it is impossible to prepare exactly the same sample having the same initial fabric for each experimental test. Besides, there may have uncertainty in the reliability of the experimental data when complex stress paths are considered.

These experimental limitations, noted above, can be avoided in the numerical experiments by DEM [8], because it enables one to prepare exactly the same sample in each numerical experiment for a certain b value without any bias in the initial fabric. In spite of the fact, limited DEM based studies were reported in the literature that considered b. For example, Thornton [9] considered the effect of σ_2 in DEM based studies and indicated that the simulated data support

the failure criterion proposed by Lade and Duncan [10]. His simulated results also depicted that the average ratio of sliding contact and the critical mechanical average coordination number are independent of b. Ng [11] reported that the models by Ogawa et al. [12] and Lade [13,14] are better than those by Satake [15] and Matsuoka and Nakai [16] for constant b-tests using DEM. In a separate study, Ng [17] indicated that the tendency of the ϕ-b relationship is not affected by the density of sample for different stress paths. In a recent study, Thornton [18] reported the stress and fabric response envelops for different deviatoric strain amplitudes using DEM.

Despite of several studies, many important experimental observations including the evolution of principal deviatoric strains and strain increment vectors under more general stress conditions defined by the parameter b have not been clarified in earlier DEM based studies. Recently, Sazzad et al. [19] reported the evolution of principal deviatoric strains and strain increment vectors for different b values under stress controlled condition in a dense sample using DEM. Nevertheless, these behaviors for a loose sample were not studied and the simulations were presented for stress controlled condition. Consideration of stress controlled constant mean stress b-test provides the opportunity to observe the simulated behavior upto peak stress state only and the post peak behavior remains unexplored. Accordingly, the current study considers the strain controlled constant mean stress b-test instead of the stress controlled constant mean stress b-test for both dense and loose samples to examine different macro features such as the evolution of principal deviatoric strains, strain increment vectors, their behavior on the normalized π-plane, etc. and different micro features such as the evolution of micro structure and fabric under more general stress conditions defined by the parameter b. To simulate the strain controlled constant mean stress b-test, the existing computer code OVAL [20] has been modified. Twelve constant mean stress true triaxial tests have been simulated in drained condition considering both the dense and loose samples by varying the b values from 0 to 1. The digital data have been analyzed and the numerical results have been reported.

2 Numerical simulations

In the current study, DEM [8] is used to carry out the numerical simulations. In DEM, Newton's second law of motion is used to calculate the motion of a particle resulting from the forces acting on the particle, while the force displacement law is used to compute the contact force from the displacement. A Coulomb type friction law is incorporated for the relative slippage between particles. For details of DEM, readers are referred to Cundall and Strack [8]. To investigate the macro- and micro-behavior of granular materials under different b values, two types of sample were prepared: (1) dense sample and (2) loose sample. To designate a sample to be dense or loose, the procedure reported by Thornton [9] were used, in which a sample density was controlled by varying the interparticle friction coefficient during the preparation of the isotropically compressed samples. To prepare the cube shaped dense and loose samples, 8,000 spheres of 16 different sizes (the diameters vary from 3 to 4.5 mm) were used. Although spheres do not strictly represent the soil particles in nature, the use of spheres as particles reduces the computational cost of simulation, in particular, when a large number of particles are considered. Preparation of a granular sample by compression method usually requires two phases: sample generation and isotropic compression. In the first phase, the spheres were placed in the grid points of known coordinates in a cubic frame, where the diameters of spheres were chosen randomly.

Table 1 Characteristics of the isotropically compressed samples

Sample designation	Void ratio	Coordination number	Length of the cubical sample (meter)
Dense	0.57	5.94	0.071
Loose	0.72	4.09	0.073

In the second phase, the isotropically compressed sample was prepared by compressing the generated sample using the periodic boundaries. To prepare an isotropically compressed dense sample, the interparticle friction coefficient μ was assigned zero, while μ was assigned 0.5 to prepare an isotropically compressed loose sample. It should be noted that the same value of μ (i.e., μ= 0.5) was used in all the subsequent shear deformations. Both the samples were compressed isotropically to 100 kPa. The characteristics of two samples are presented in Table 1, where the coordination number is defined as twice the total number of contacts divided by the total number of particles. A cube with principal stress directions is depicted in Fig. 1a, while the configuration of the isotropically compressed dense sample is depicted in Fig. 1b, for example.

Twelve mean stress controlled true triaxial tests were carried out using the dense and loose numerical samples in drained condition for different b values ranging from 0 (axisymmetric triaxial compression) to 1 (axisymmetric triaxial extension). The isotropically compressed dense and loose samples (Table 1) were subjected to strain controlled triaxial shear deformation according to the given value of b by keeping the mean stress constant (100 kPa). In the strain controlled constant mean stress b-test simulation, the sample height was reduced slowly downward with a very small and constant strain increment of 2.0×10^{-5} % in each time step, while the lateral stresses are continuously adjusted

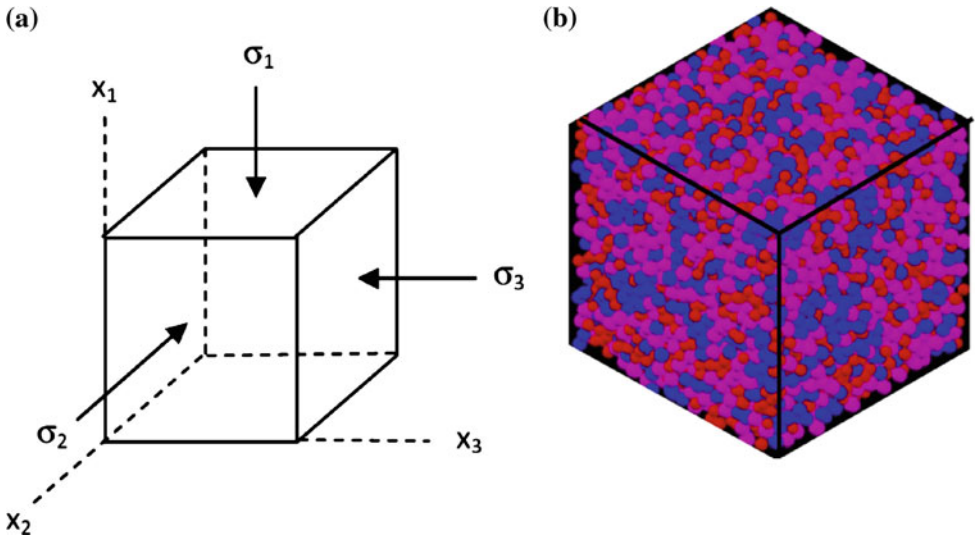

Fig. 1 **a** A cubic element with principal stress directions and reference axes. **b** Configuration of the isotropically compressed dense sample

Table 2 Simulation parameters and conditions

Simulation parameters and conditions	Value
Normal contact stiffness (N/m)	1×10^6
Tangential contact stiffness (N/m)	1×10^6
Mass density (kg/m^3)	2,650
Increment of time step (s)	1×10^{-6}
Interparticle friction coefficient (μ)	0.5
Dimensionless coefficient of viscosity for translational and rotational body damping	0.05
Method of simulation	Strain controlled

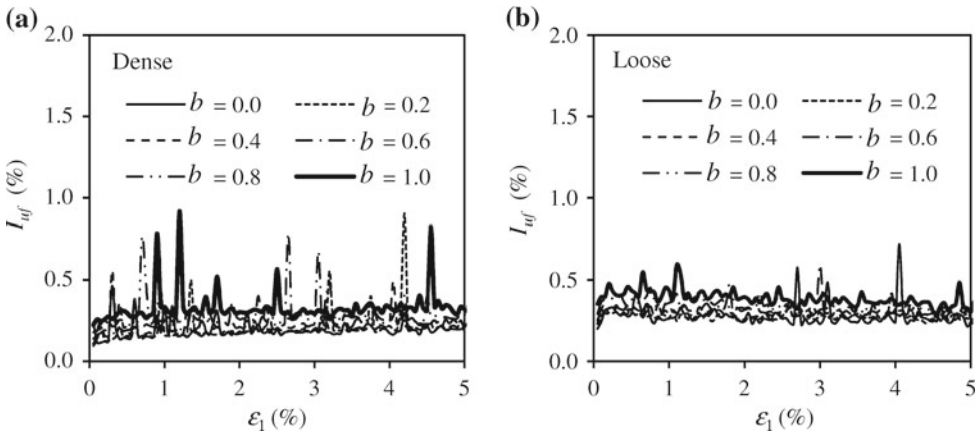

Fig. 2 Evolution of I_{uf} with ε_1. **a** For dense sample. **b** For loose sample

by regulating the lateral system dimensions to maintain the given mean stress and b value throughout the simulation. The vertical stress (σ_1) is measured and via σ_1, other stresses (σ_2 and σ_3) are computed such that the mean of the stresses (σ_1, σ_2 and σ_3) remains constant and given b is maintained. The same DEM parameters (Table 2) were used for all the simulations. To examine the quasi-static condition, the evolution of index I_{uf} is recorded and plotted against the major principal strain ε_1 and depicted in Fig. 2. The index I_{uf} is defined as follows [21]:

$$I_{uf} = \sqrt{\frac{\sum_{1}^{N_p} (unbalanced\ forces)^2/N_p}{\sum_{1}^{N_c} (contact\ forces)^2/N_c}} \times 100\,(\%), \qquad (1)$$

where N_p represents the number of particles and N_c represents the number of contacts. The unbalanced force in Eq. (1) is defined as the resultant force acting through the centroid of a particle. A small value of I_{uf} is desirable, because it is associated with the higher simulation accuracy [20,21]. As seen

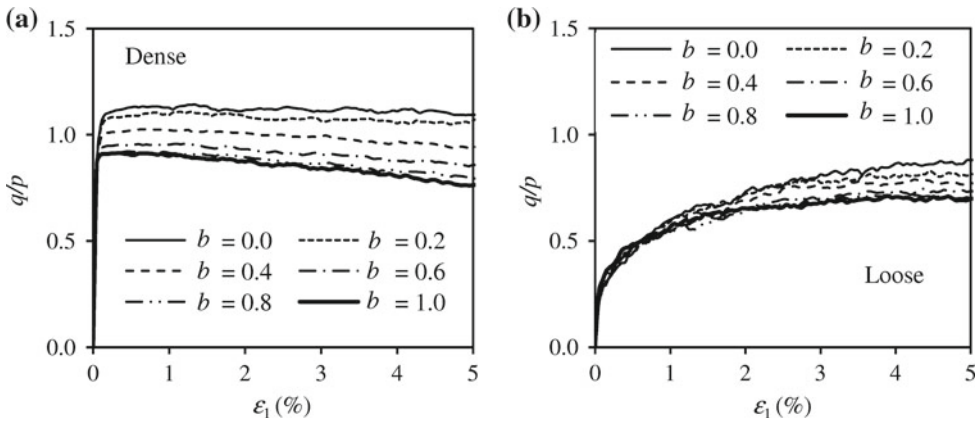

Fig. 3 Stress-strain relationship for different b values. **a** For dense sample. **b** For loose sample

in Fig. 2, I_{uf} remains very small throughout the simulation regardless of b and the density of sample.

3 Numerical results

3.1 Stress-strain-dilative response

Figure 3 depicts the simulated stress-strain behavior of granular materials for different b values (0, 0.2, 0.4, 0.6, 0.8, and 1) using both the dense and loose samples. The stress ratio q/p attains an earlier peak followed by strain softening for dense sample, while the same for loose sample gradually increases until it reaches the peak value regardless of b. Here, the mean stress p is defined as $p = (\sigma_1 + \sigma_2 + \sigma_3)/3$ and the equivalent deviatoric stress q is defined as $q = \sqrt{3\{(\sigma_1 - p)^2 + (\sigma_2 - p)^2 + (\sigma_3 - p)^2\}/2}$. The evolution of q/p is strongly influenced by the variations of b regardless of the density of sample. The relationship between the friction angle ϕ at peak stress ratio and b for dense and loose samples is depicted in Fig. 4. It is clear that ϕ increases up to a certain value of b regardless of the density of sample and beyond the peak value, ϕ decreases when b approaches unity. This tendency agrees qualitatively with the experimental observation for dense sample (e.g., [2,6,22]) and for loose sample (e.g., [4]). The same tendency was also reported in a very recent DEM based study by Sazzad et al. [19] for dense sample under stress controlled simulation condition.

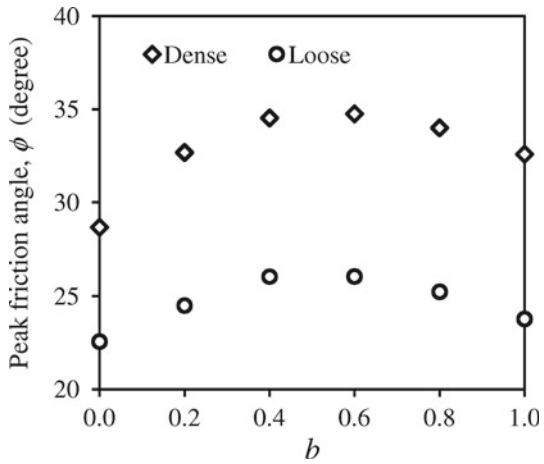

Fig. 4 ϕ-b relationship for dense and loose samples

Figure 5 depicts the relationship between the stress ratio and volumetric strain for different b values and sample densities. The volumetric strain in Fig. 5 is defined as $\varepsilon_V = \varepsilon_1 + \varepsilon_2 + \varepsilon_3$, where $\varepsilon_1, \varepsilon_2$ and ε_3 are the major, intermediate and minor principal strains, respectively. A positive value of ε_V indicates compression, while a negative value

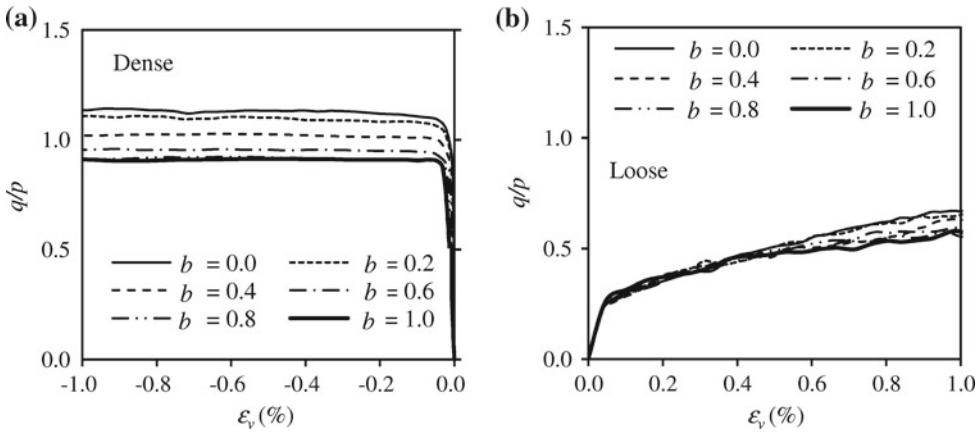

Fig. 5 Relationship between stress ratio and volumetric strain for different b values. **a** For dense sample. **b** For loose sample

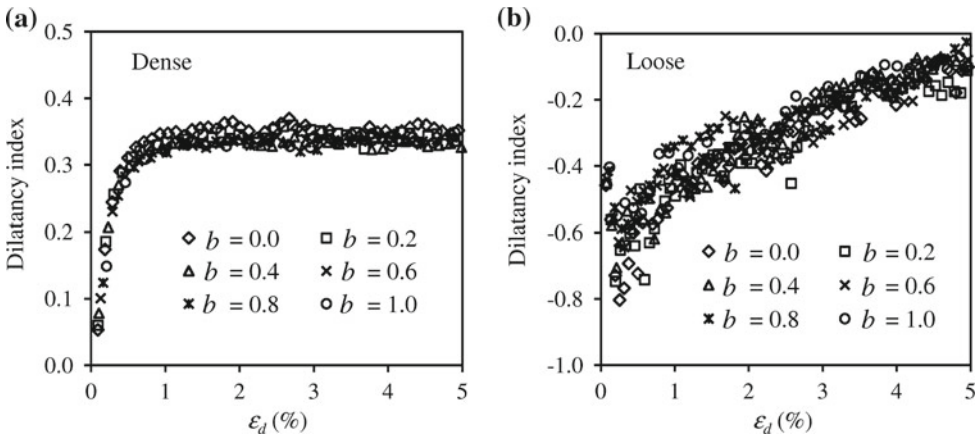

Fig. 6 Relationship between dilatancy index and equivalent deviatoric strain for different b values. **a** For dense sample. **b** For loose sample

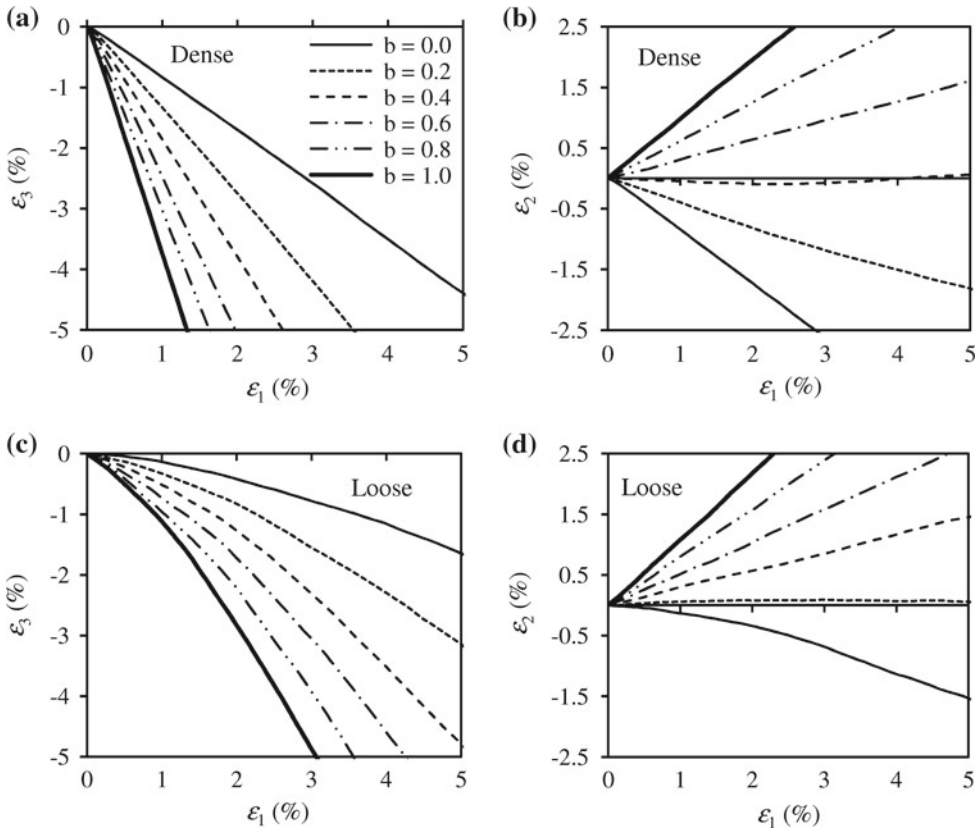

Fig. 7 Evolution of minor and intermediate principal strains with major principal strain under different b values. **a** ε_3 versus ε_1 for dense sample. **b** ε_2 versus ε_1 for dense sample. **c** ε_3 versus ε_1 for loose sample. **d** ε_2 versus ε_1 for loose sample

indicates dilation. Note that dilation prevails in dense sample, while compression prevails in loose sample. The DEM results, presented in Fig. 5, are qualitatively comparable with the experimental results reported by Suzuki and Yanagisawa [23]. The evolution of dilatancy index with the equivalent deviatoric strain ε_d is depicted in Fig. 6. The equivalent deviatoric strain and the dilatancy index are defined as $\varepsilon_d = \sqrt{2\{(\varepsilon_1-\varepsilon_2)^2+(\varepsilon_2-\varepsilon_3)^2+(\varepsilon_3-\varepsilon_1)^2\}/3}$ and $DI = -d\varepsilon_V/d\varepsilon_d$, where $d\varepsilon_V$ is the change in volumetric strain and $d\varepsilon_d$ is the change in equivalent deviatoric strain. The relationship between dilatancy index and ε_d depicts a unique behavior for small strain level regardless of b for dense sample, while the same for loose sample is not unique. Figure 7 depicts the evolution of ε_3 and ε_2 with ε_1 for dense and loose samples, while Fig. 8 depicts the evolution of e_3 and e_2 with e_1 for dense and loose samples, where e_1, e_2 and e_3 are the major, intermediate and minor principal deviatoric strains, respectively. The principal deviatoric strains are given by $e_1 = \varepsilon_1 - \varepsilon_m$, $e_2 = \varepsilon_2 - \varepsilon_m$ and $e_3 = \varepsilon_3 - \varepsilon_m$, where $\varepsilon_m = (\varepsilon_1+\varepsilon_2+\varepsilon_3)/3$. The relationships among principal strains are non-linear and this is more obvious in loose sample than dense sample.

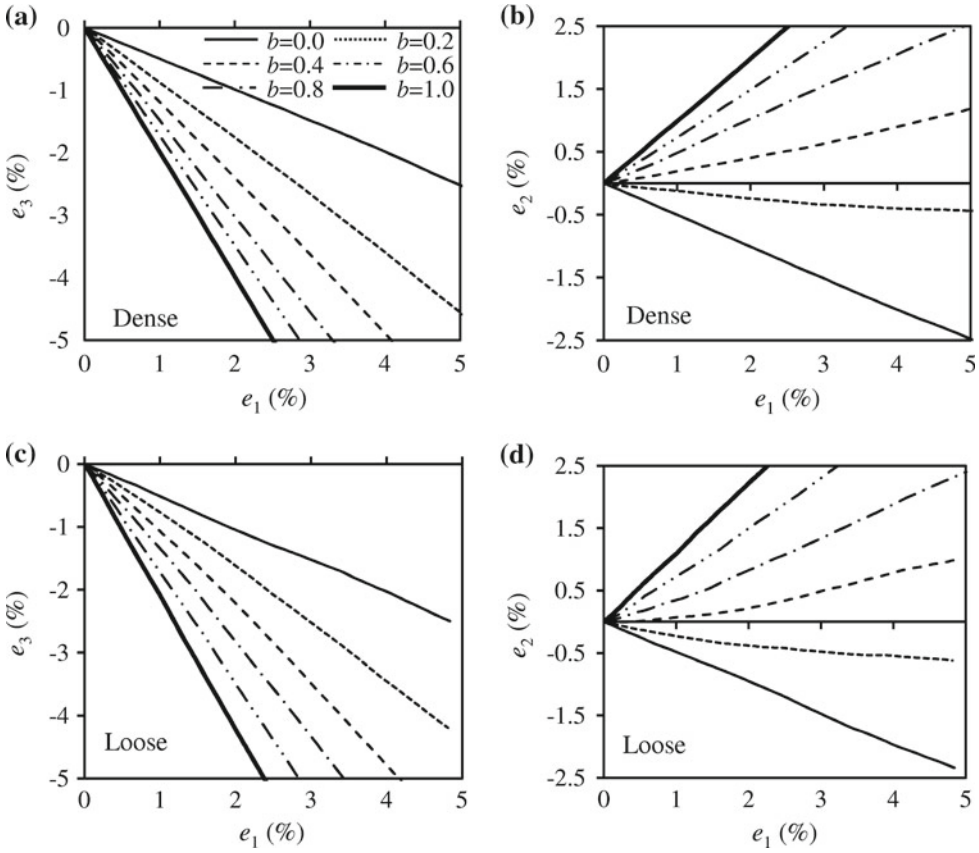

Fig. 8 Evolution of minor and intermediate principal deviatoric strains with the major principal deviatoric strain under different b values. **a** e_3 versus e_1 for dense sample. **b** e_2 versus e_1 for dense sample. **c** e_3 versus e_1 for loose sample. **d** e_2 versus e_1 for loose sample

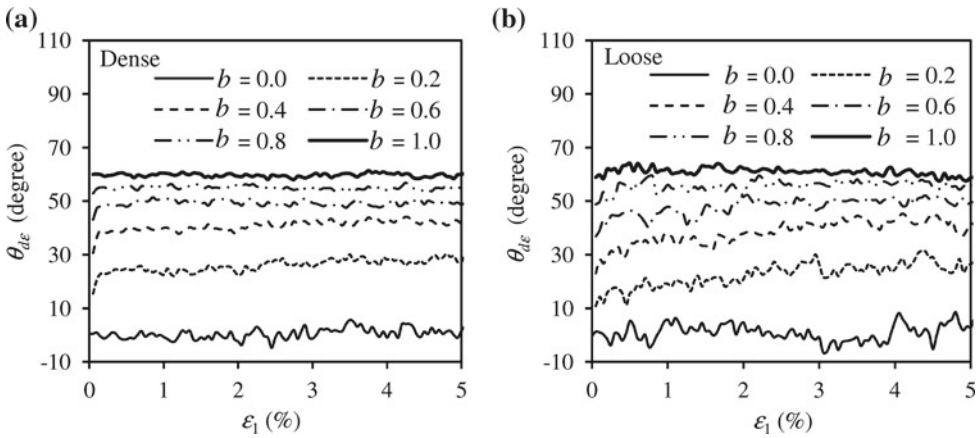

Fig. 9 Evolution of strain increment vector direction with ε_1 under different b values. **a** For dense sample. **b** For loose sample

3.2 Strain increment vector

The evolution of strain increment vector direction for different b values with ε_1 is depicted in Fig. 9. The angle between the principal strain increment vector and the maximum strain increment axis can be expressed as follows [23]:

$$\theta_{d\varepsilon} = \tan^{-1}\left[\frac{\sqrt{3}b_{d\varepsilon}}{2 - b_{d\varepsilon}}\right], \tag{2}$$

$$\text{where } b_{d\varepsilon} = \frac{d\varepsilon_2 - d\varepsilon_3}{d\varepsilon_1 - d\varepsilon_3} \tag{3}$$

It is noted in Fig. 9 that $\theta_{d\varepsilon}$ diverts from its initial value as ε_1 increases. Dominant change in $\theta_{d\varepsilon}$ is noticed for the intermediate values of b. It should also be noted that the change in $\theta_{d\varepsilon}$ is more irregular for loose sample compared to dense sample.

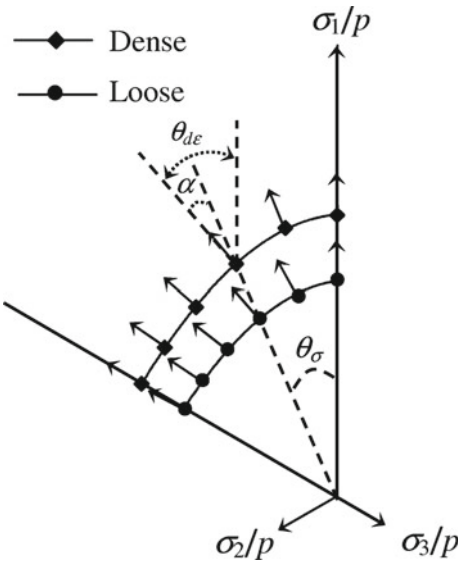

Fig. 10 Unit vector of strain increment superimposed on the normalized π-plane at the peak stress ratio of the stress-strain curve

3.3 Failure surface

Figure 10 depicts the failure surface on the normalized π-plane (normalized by the mean stress p) at the peak stress ratio for dense and loose samples. The strain increment vectors are superimposed on the failure surface to investigate their evolution for different values of b. Note that $\theta_{d\varepsilon}$ has nearly the same direction to that of stress vector θ_σ for b= 0 and 1, while a divergence is noticed for the intermediate values of b regardless of the density of sample. The stress vector direction θ_σ, which is the angle between the principal stress vector and the maximum principal stress axis, can be related to b by the following expression:

$$\theta_\sigma = \tan^{-1}\left[\frac{\sqrt{3}b}{2-b}\right] \tag{4}$$

Note also that the strain increment vector directions are not normal to the failure surfaces on the normalized π-plane for some values of b.

A comparison of the simulated results by DEM with the failure criteria proposed by Lade and Duncan [10] and Matsuoka and Nakai [24] is depicted in Fig. 11. The failure criteria by Lade and Duncan [10] and Matsuoka and Nakai [24] are given in Eqs. (5) and (6), respectively.

$$\frac{I_1^3}{I_3} = k_1, \tag{5}$$

$$\frac{I_1 I_2}{I_3} = 8\tan^2\phi_p + 9 = k_2, \tag{6}$$

where I_1, I_2 and I_3 are the first, second and third stress invariants of the stress tensor, respectively and k_1 is the material parameter for Lade and Duncan's [10] failure criterion, ϕ_p is the peak friction angle in triaxial compression and $k_2 = 8\tan^2\phi_p + 9$ for Matsuoka and Nakai's [24] failure criterion. For Lade and Duncan's [10] model, k_1 is first calculated for $b = 0$ with the known values of σ_1, σ_2, σ_3 at the peak stress ratio using Eq. (5) and later, the same value of k_1 is used to determine σ_1, σ_2, σ_3 for other values of b using Eq. (5). A similar procedure is used for Matsuoka and Nakai's [24] model. $k_2 = 8\tan^2\phi_p + 9$ is determined for b= 0 and the same value of k_2 is used in Eq. (6) to obtain σ_1, σ_2, σ_3 for other values of b. Note that Lade and Duncan's [10] failure model approximates the DEM based failure surface better than that of Matsuoka and Nakai's [24] for dense sample. This tendency has also been reported in the earlier DEM based studies [17–19,31] for dense sample. In the current study, we notice that both the models approximate the DEM based failure surface reasonably well when loose samples are considered.

As noticed in Fig. 10, a deviation between $\theta_{d\varepsilon}$ and θ_σ remains for the intermediate values of b. This deviation angle can be expressed as $\alpha = \theta_{d\varepsilon} - \theta_\sigma$. The relationship between

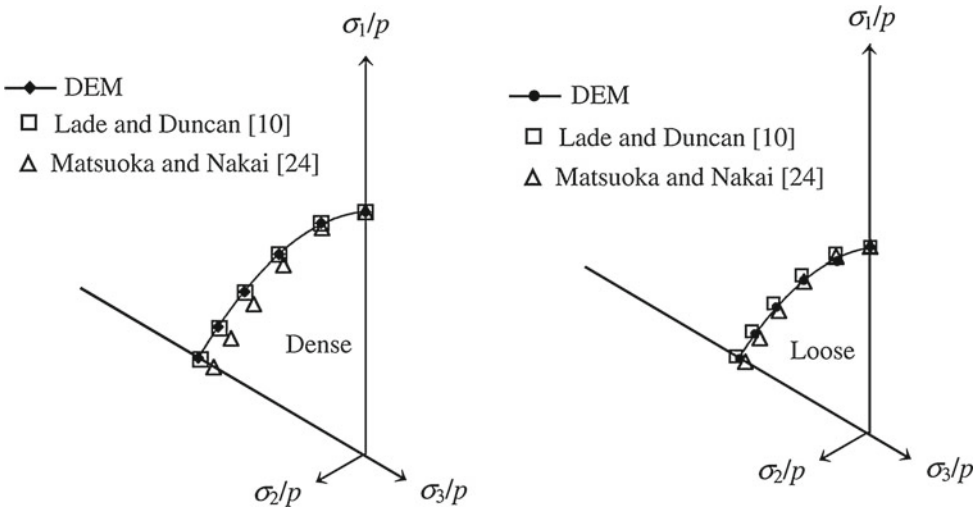

Fig. 11 Comparison of the DEM data against Lade and Duncan's [10] and Matsuoka and Nakai's [24] failure criteria for dense and loose samples

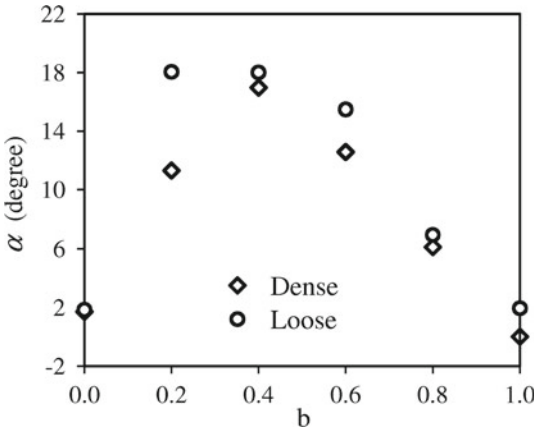

Fig. 12 Relationship between deviation angle α and b value at the peak stress level for dense and loose samples

α and b is depicted in Fig. 12 for dense and loose samples. Note that α is not zero for both $b = 0$ and $b = 1$ though axisymmetry entails α to be zero for both $b = 0$ and $b = 1$. Any departure from these values is due to disorder (a finite sample does not exactly abide by the axial symmetry). In Fig. 12, it is clear that α is dependent on the intermediate values of b. α is maximum for $b = 0.4$ in case of dense sample, while α is maximum for $b = 0.2$ in case of loose sample.

It is observed from the numerical simulation (see Fig. 7) that the near plane strain condition is obtained for $b = 0.4$ in case of dense sample, while the near plane stain condition is obtained for $b = 0.2$ in case of loose sample. This reveals that α is maximum near the plane strain condition of the simulation.

3.4 Micro scale variables

Figure 13a depicts the relationship between the coordination number and b, while Fig. 13b depicts the relationship between the sliding contact fraction in percentage and b at the peak stress state for dense and loose samples. To study the sensitivity of the measured values of coordination number and sliding contact fraction to strain increment, we have simulated additional twenty four constant mean stress b-tests for other two strain increments of 1.0×10^{-5} % and 4.0×10^{-5} % in each time step for both the dense and loose samples and the measured values are depicted in the same Figs. (i.e., Fig. 13a, b). Sliding contact fraction is defined here as the total number of sliding contacts divided by the total number of contacts at a given state of simulation. The evolution of coordination number and sliding contact fraction with the variation of b has also been reported in the earlier

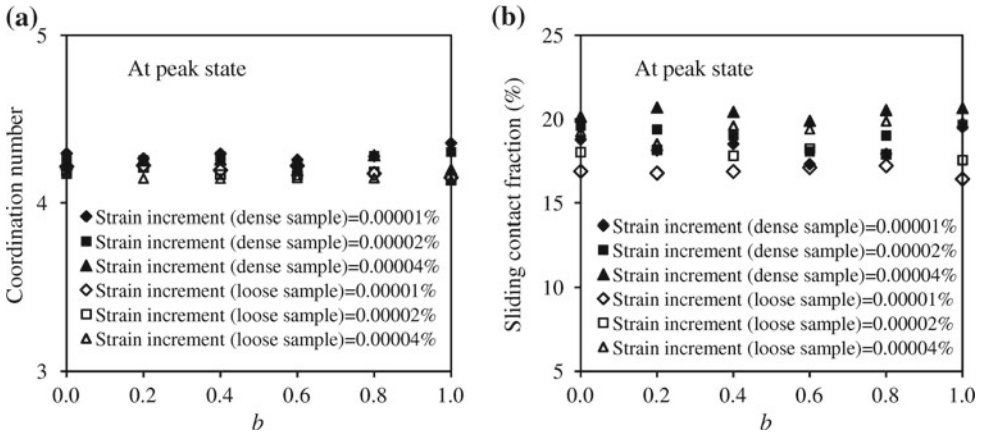

Fig. 13 **a** Relationship between coordination number and b for dens e and loose sample at peak stress ratio. **b** Relationship between sliding contact fraction and b for dense and loose sample at peak stress ratio

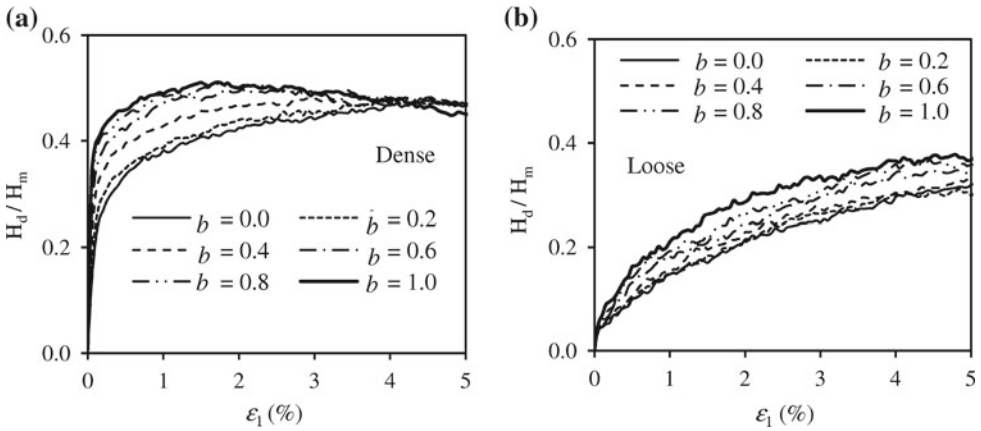

Fig. 14 Relationship between H_d/H_m and ε_1 for different b considering all contacts. **a** For dense sample. **b** For loose sample

DEM based studies (e.g., [9,19]) for a certain value of strain or stress increment. These studies depicted that coordination number is independent of the stress path for dense sample defined by the parameter b. In the current study, it is noted that the evolution of coordination number is little susceptible to the variation of b at the peak stress state regardless of the density of sample and increment of strain. However, the evolution of sliding contact fraction is found to have a bit susceptibility to the density of sample and increment of strain for the variation of b at the peak stress state.

3.5 Macro-micro relationship

One of the goals of the researchers in DEM based studies is to relate the micro quantities with the macro quantities [19,25–27,29,30,32–36,38] among others]. Several approaches have been noticed in the literature to relate the stress ratios quantitatively with fabric and force distribution anisotropies. For example, in several studies, the stress ratio was related to the anisotropies developed from contact normal vector, normal contact force and tangential contact force (e.g., [25,30,32,36]). In contrast to the previous approach, several studies related the stress ratio to a single parameter computed from the contact normal vectors (e.g., [17,27,33,34]). The studies, referred above, were carried out in 2D for biaxial compression (e.g., [25,30,27]) and 3D for axisymmetric triaxial compression (i.e, for $b = 0$) (e.g., [32–34,36]). Nevertheless, these relationships for other values of b are limited in the literature. Among these limited studies, Ng [26] and Sazzad et al. [19] correlated the macro and micro quantities for different values of b. Ng [26] indicated that obliquity relates better with the microscopic parameter related to the contact normal force than with the unit normal vector for different stress paths. By contrast, Sazzad et al. [19] reported that a unique macro-micro relationship exists between the stress ratio and the deviatoric fabric related to the unit normal vector of strong contacts for different b values under stress controlled simulation condition in a dense sample. Although these studies considered different values of b, loose samples were not considered. In the current study, an attempt has also been made similar to the approaches taken in [33,34] to establish a linkage between the macro and micro quantities under strain controlled simulation condition for various values of b ranging from 0 to 1 considering both the dense and loose samples. With this view, a fabric tensor is defined considering all contacts in the simulation as follows [28]:

$$H_{ij} = \frac{1}{N_c} \sum_{c=1}^{N_c} n_i^c n_j^c, \tag{7}$$

where n_i^c is the i-th component of the unit normal vector at c-th contact; N_c is the total number of contacts in the assembly. The total contact can be further divided into strong contact and weak contact. The distinction of "strong" force networks and it relation to stress anisotropy was introduced in [30]. In the current study, a fabric tensor for strong contacts is defined as follows:

$$H_{ij}^s = \frac{1}{N_c} \sum_{s=1}^{N_s} n_i^s n_j^s, \tag{8}$$

where n_i^s is the i-th component of the unit normal vector at the s-th strong contact, N_s is the number of strong contacts. A contact is said to be strong if it carries a normal contact force greater than the average normal contact force. The average normal contact force is defined here as follows:

$$f_{ave}^n = \frac{1}{N_c} \sum_{i=1}^{N_c} f_i^n, \tag{9}$$

where f_i^n is the i-th normal contact force.

Figure 14 depicts the evolution of fabric measure H_d/H_m with ε_1 for dense and loose samples considering all contacts. We have defined H_d and H_m similar to q and p as follows: $H_d = \sqrt{3\{(H_{11}-H_m)^2+(H_{22}-H_m)^2+(H_{33}-H_m)^2\}/2}$ and $H_m = (H_{11} + H_{22} + H_{33})/3$. Although the shape of H_d/H_m versus ε_1 curve has little similarity with q/p versus ε_1 curve, the tendency is different. For example, the stress ratio q/p is minimum when b is 1, while the fabric measure H_d/H_m is maximum when b is 1. Instead, the evolution of fabric considering the strong contacts can be considered. The evolution of fabric measure H_d^s/H_m^s considering the strong contacts with ε_1 for dense and loose samples is depicted in Fig. 15, where H_d^s and H_m^s are defined as follows: $H_d^s = \sqrt{3\{(H_{11}^s - H_m^s)^2 + (H_{22}^s - H_m^s)^2 + (H_{33}^s - H_m^s)^2\}/2}$ and $H_m^s = (H_{11}^s + H_{22}^s + H_{33}^s)/3$. Note that H_d^s/H_m^s versus ε_1 curve has nice similarity with q/p versus ε_1 curve for different values of b ranging from 0 to 1. Antony and Kuhn [34] also observed the similarity between the deviatoric to mean stress ratio and axial strain for axisymmetric triaxial compression ($b = 0$) in a dense sample considering strong contacts in the simulation. The current study depicts that the similarity is also available for general stress paths (i.e., for other values of b) considering only the strong contacts.

The relationship of $(H_d^s/H_m^s)_{peak}$ versus b and $(q/p)_{peak}$ versus b is depicted in Fig. 16 for dense and loose samples. The relationship between $(H_d^s/H_m^s)_{peak}$ and b has an excellent similarity with the relationship between $(q/p)_{peak}$ and b. This similarity suggests that the difference of the peak stress ratio for different b values is the consequence of the difference in the fabric anisotropy developed due to strong contacts during shear deformation. The relationship between the stress ratio q/p and fabric measure H_d^s/H_m^s is depicted in Fig. 17 for different b values and sample densities. A unique relationship between q/p and H_d^s/H_m^s is noted regardless of

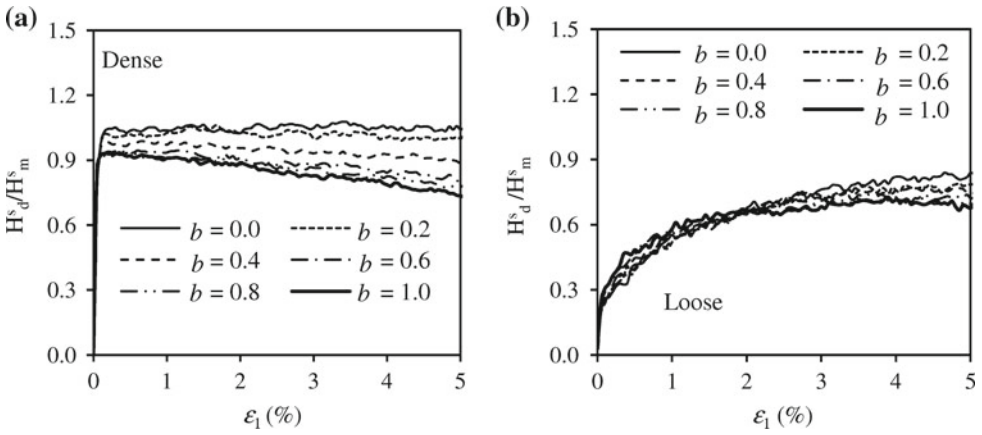

Fig. 15 Relationship between H^s_d/H^s_m and ε_1 for different b considering strong contacts. **a** For dense sample. **b** For loose sample

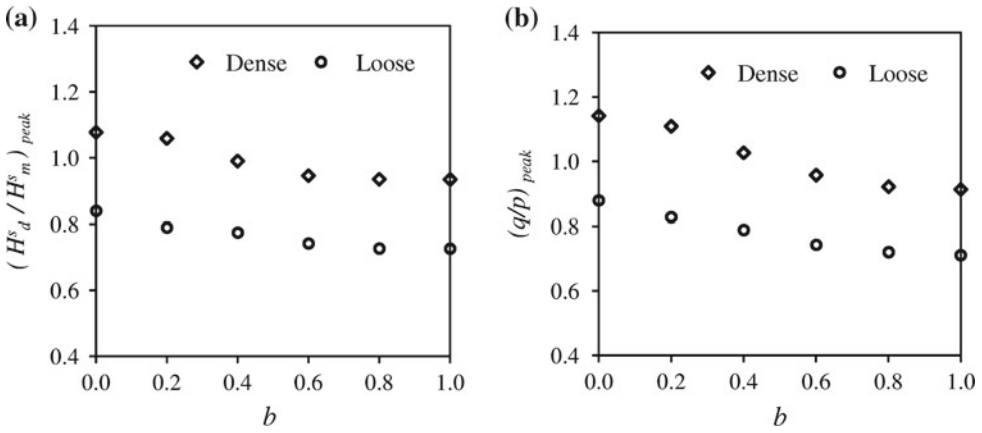

Fig. 16 **a** Relationship between $(H^S_d/H^S_m)_{peak}$ and b for dense and loose samples. **b** Relationship between $(q/p)_{peak}$ and b for dense and loose samples

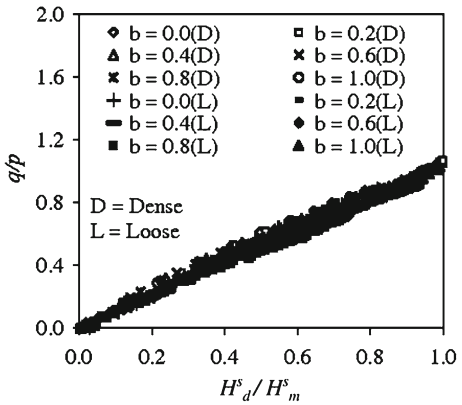

Fig. 17 Relationship between q/p and H^s_d/H^s_m for different densities and b values

b and sample densities when strong contacts are considered. Following the similar approach of the current study (i.e., considering only the fabric related to the contact normal), Antony et al. [37] depicts that the ratio of the stress ratio to the square root of fabric ratio contributed by the strong contacts is $\approx 1/2$ in a 2D biaxial simulation for oval particles. In our study, we depicts that the ratio of q/p to H^s_d/H^s_m is ≈ 1 regardless of b and sample densities.

4 Conclusions

A detailed numerical study for the comparison of different macro and micro quantities for different densities of the numerical samples and b values is presented in this paper. A series of strain controlled constant mean stress b-test were carried out without any bias in the initial fabric of the numerical dense and loose samples. The simulated stress-strain-dilative responses for different b values under dense and loose conditions of the numerical samples were in good agreement with the experimental tendencies qualitatively. Some of the points of the numerical study can be summarized as follows:

1. A unique relationship between dilatancy index and equivalent deviatoric strain is noticed for small strain level regardless of b value for dense sample, while the same for loose sample is not unique.
2. The change in strain increment vector direction is more irregular for loose sample than dense sample.
3. The Lade and Duncan's [10] failure model approximates the DEM based failure surface better than Matsuoka and Nakai's failure model [24] for dense sample, while for loose sample, both the models approximate the DEM based failure surface reasonably well.

4. The evolution of coordination number is little susceptible to the variation of b at the peak state regardless of the density of sample and increment of strain.
5. A linkage between stress ratio and fabric measure is depicted. A unique relation between the stress ratio and fabric measure related to the strong contacts is noticed regardless of b value and the density of sample.

References

1. Habib, P.: Influence of the variation of the average principal stress upon the shearing strength of soils. In: Proceedings of 3rd International Conference on Soil Mechanics and Foundation Engineering 1, pp. 131–136 (1953)
2. Ko, H.-Y., Scott, R.F.: Deformation of sand at failure. J. Soil Mech. Found. Div. ASCE **94**(4), 883–898 (1968)
3. Lade, P.V.: Cubical triaxial tests on cohesionless soil. J. Soil Mech. Found. Div. ASCE **99**(SM10), 793–812 (1973)
4. Haruyama, M.: Anisotropic deformation-strength characteristics of an assembly of spherical particles under 3-D stresses. Soils Found **21**(4), 41–55 (1981)
5. Lam, W.-K., Tatsuoka, F.: Effects of initial anisotropic fabrics and σ_2 on strength and deformation characteristics of sand. Soils Found **28**(1), 89–106 (1988)
6. Wang, Q., Lade, P.V.: Shear banding in true triaxial tests and its effect on failure in sand. J. Eng. Mech. ASCE **127**(8), 754–761 (2001)
7. Sun, D., Huang, W., Yao, Y.: An experimental study of failure and softening in sand under three-dimensional stress condition. Granul. Matter **10**(3), 187–195 (2008)
8. Cundall, P.A., Strack, O.D.L.: A discrete numerical model for granular assemblies. Geotechnique **29**(1), 47–65 (1979)
9. Thornton, C.: Numerical simulations of deviatoric shear deformation of granular media. Geotechnique **50**(1), 43–53 (2000)
10. Lade, P.V., Duncan, J.M.: Elastoplastic stress-strain throry for cohesionless soil. J. Geotech. Eng. Div. **101**(10), 1037–1053 (1975)
11. Ng, T.-T.: Shear strength of assemblies of ellipsoidal particles. Geotechnique **54**(10), 659–669 (2004)
12. Ogawa, S., Mitsui, S., Takemure, O.: Influence of intermediate principal stress on mechanical properties of a sand. In: Proceedings of 29th Annual Meeting of JSCE, Part 3, pp. 49–50 (1974)
13. Lade, P.V.: Elasto-plastic stress-strain theory for cohesionless soil with curved yield surfaces. Int. J. Solids Struct. **13**(11), 1019–1035 (1977)
14. Lade, P.V.: Failure criterion for frictional materials. In: Desai, C.S., Gallagher, R.H. (eds.) Mechanics of Engineering Material, pp. 385–402. Wiley, New York (1984)
15. Satake, M.: Consideration of yield criteria from the concept of metric space. Technol. Rep. Tohoku Univ. **40**(2), 521–530 (1975)
16. Matsuoka, H., Nakai, T.: A generalized frictional law of soil shear deformation. In: Proceedings of US-Japan Seminar on Continuum-mechanical and Statistical Approaches in Mechanics of Granular Materials, Tokyo, pp. 138–154 (1978)
17. Ng, T.-T.: Behavior of gravity deposited granular material under different stress paths. Can. Geotech. J. **42**(6), 1644–1655 (2005)
18. Thornton, C.: Quasi-static simulations of compact polydisperse particle systems. Particuology **8**(2), 119–126 (2010)
19. Sazzad, M.M., Suzuki, K., Modaressi-Farahmand-Razavi, A.: Macro-micro responses of granular materials under different b values using DEM. Int.l J. Geomech. ASCE **12**(3), 220–228 (2012)
20. Kuhn, M.R.: OVAL and OVALPLOT: Programs for analyzing dense particle assemblies with the discrete element method". http://faculty.up.edu/kuhn/oval/doc/oval_0618.pdf (2006). Last Accessed 9 July 2012
21. Ng, T.-T.: Input parameters of discrete element methods. J. Eng. Mech. ASCE **132**(7), 723–729 (2006)
22. Ergun, M.U.: Evaluation of three-dimensional shear testing. In: Proceedings of 10 th International Conference on Soil Mechanics and Foundation Engineering, Stockholm, Sweden, 1, pp. 593–596 (1981)
23. Suzuki, K., Yanagisawa, E.: Principal deviatoric strain increment ratios for sand having inherent transverse isotropy. Int. J. Geomech. ASCE **6**(5), 356–366 (2006)
24. Matsuoka, H., Nakai, T.: Stress-deformation and strength characteristics of soil under three difference principal stresses. In: Proceedings of JSCE, 232, 59–70 (1974)
25. Rothenburg, L., Bathurst, R.J.: Analytical study of induced anisotropy in idealized granular materials. Geotechnique **39**(4), 601–614 (1989)
26. Ng, T.-T.: Macro- and micro-behaviors of granular materials under different sample preparation methods and stress paths. Int. J. solids. Struct. **41**(21), 5871–5884 (2004)
27. Sazzad, M.M., Suzuki, K.: Effect of interparticle friction on the cyclic behavior of granular materials using 2D DEM. J. Geotech. Geoenviron. Eng. ASCE **137**(5), 545–549 (2011)
28. Satake, M.: Fabric tensor in granular materials. In: Vermeer P.A., Luger H.J. (eds.) Proceedings IUTAM Symposium on Deformation and Failure of Granular Materials, Delft, Balkema, pp. 63–68 (1982)
29. Luding, S., Lätzel, M., Volk, W., Diebels, S., Herrmann, H.J.: From discrete element simulations to a continuum model. Comput. Methods Appl. Mech. Engrg. **191**(1), 21–28 (2001)
30. Radjai, F., Wolf, D.E., Jean, M., Moreau, J.J.: Bimodal character of stress transmission in granular packings. Phys. Rev. Letter **80**, 61–64 (1998)
31. Suiker, A.S.J., Fleck, N.A.: Frictional collapse of granular assemblies. J. Appl. Mech. ASME **71**(3), 350–358 (2004)
32. Azéma, E., Radjai, F., Peyroux, R., Saussine, G.: Force transmission in a packing of pentagonal particles. Phys. Rev. E **76**(1), 01130 (2007)
33. Antony, S.J.: Evolution of force distribution in three-dimensional granular media. Phys. Rev. E **63**(1), 011302 (2001)
34. Antony, S.J., Kuhn, M.R.: Influence of particle shape on granular contact signatures and shear strength: new insights from simulations. Int. J. Solids Struct. **41**(21), 5863–5870 (2004)
35. Azéma, E., Radjai, F., Saussine, G.: Quasistatic rheology, force transmission and fabric properties of a packing of irregular polyhedral particles. Mech. Mater. **41**(6), 729–741 (2009)
36. Ouadfel, H., Rothenburg, L.: 'Stress-force-fabric' relationship for assemblies of ellipsoids. Mech. Mater. **33**(4), 201–221 (2001)
37. Antony, S.J., Momoh, R.O., Kuhn, M.R.: Micromechanical modelling of oval particulates subjected to bi-axial compression. Computa. Mater. Sci. **29**(4), 494–498 (2004)
38. Alonso-Marroquin, F., Luding, S., Herrmann, H.J., Vardoulakis, I.: Role of the anisotropy in the elastoplastic response of a polygonal packing. Phys. Rev. E **71**, 051304 (2005)